Insight into the adsorption of europium(III) on muscovite and phlogopite: Effects of pH, electrolytes, humic substances and mica structures

Hanyu WU[a], Jie CHEN[a,†], Zengbo SU[b,†], Bin MA[c], Yizhe JI[a], Shuhan LIN[a], Dingfang XU[a], Mingliang KANG[a,*]

[a] Sino-French Institute of Nuclear Engineering and Technology, Sun Yat-sen University, Zhuhai 519082, China

[b] Fujian Fuqing Nuclear Power Co., Ltd., Fuqing 350300, China

[c] Empa, Swiss Federal Laboratories for Materials Science and Technology, Dübendorf, Switzerland

[†] Authors contributed equally to this work.

[*] Corresponding authors: Mingliang KANG

E-mail: kangml3@mail.sysu.edu.cn,

Address: Sino-French Institute of Nuclear Engineering and Technology, Sun Yat-sen University, Zhuhai 519082, China.

Tel.: +86 756 3668392

This document is the accepted manuscript version of the following article:
Wu, H., Ma, B., Chen, J., Su, Z., Ji, Y., Lin, S., … Kang, M. (2021). Insight into the adsorption of europium(III) on muscovite and phlogopite: effects of pH, electrolytes, humic substances and mica structures. Chemosphere, 282, 131087 (10 pp.). https://doi.org/10.1016/j.chemosphere.2021.131087

Abstract

Europium(III), i.e., Eu(III), is chemically analogous to the trivalent lanthanides (Ln) and actinides (An). A good understanding of the adsorption behaviour of Eu(III) on mica group minerals is critical to the safety evaluation of the radioactive contamination. Nevertheless, the structural complexity of micaceous minerals makes it difficult to draw a consistent conclusion in the study of Eu(III) migration. In this work, we contrastively studied Eu(III) adsorption on dioctahedral muscovite and trioctahedral phlogopite as functions of pH, ionic strength, background electrolytes, interaction sequence, and fulvic acid (FA). Batch experiments showed that Eu(III) adsorption on both micas was strongly dependent on pH but quite independent on ionic strength that is determined by Na^+. Planar sites are available on both muscovite and phlogopite while interlayer sites only on phlogopite under Na^+ and Ca^{2+} electrolytes (not for K^+ and Cs^+). An interlayer expansion of phlogopite, as indicated by a newly appeared diffraction peak at ~6^o 2-theta, occurred along with Eu(III) adsorption, which was also confirmed by transmission electron microscopy. Furthermore, the initial Eu(III) concentrations, the concentration ratios between Eu(III) and Cs^+, and the reaction sequences of Eu(III)-electrolytes-FA affected both the adsorption behaviour of Eu(III) and reversely the structural alteration of phlogopite. The sequential extraction showed that the adsorbed Eu(III) was mainly in the ion-exchangeable form while the addition of FA could increase the portion of coordinative species. The currently proposed Eu(III) adsorption mechanism can shed new light on predicting the migration of Ln/An(III) at the mica-rich solid-liquid

39 interface on a molecular scale.

40 **Keywords**

41 Adsorption, Europium, Muscovite, Phlogopite, Fulvic acid

42 **Graphical abstract**

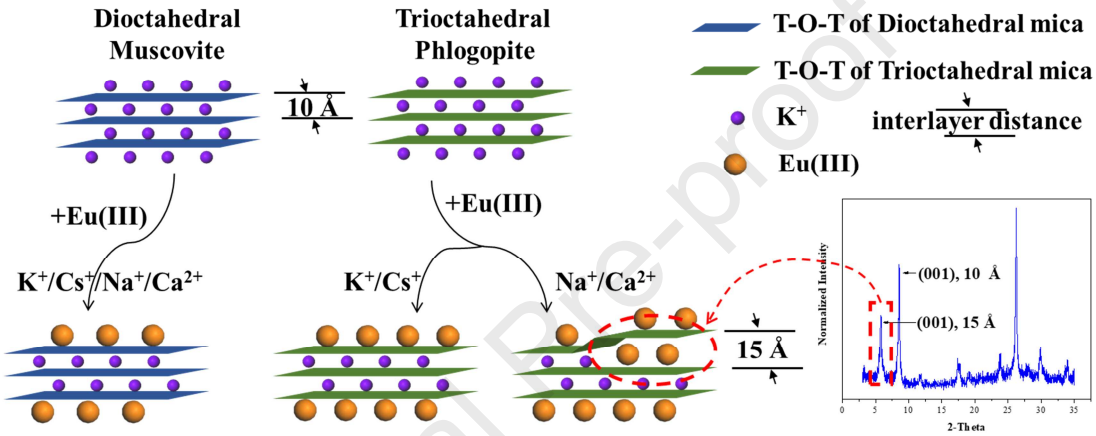

43

44

1 Introduction

The retention of radionuclides by the natural geosphere, in particular in the vicinity of nuclear waste temporary storage or repositories, is considered a critical and last pathway of radionuclides stabilization and also an ongoing concern for safety assessment of the repository and environmental research (Ma et al., 2020; Niu et al., 2009; Sun et al., 2020; Zhang et al., 2020). The geological fate of radionuclides in the environment greatly depends on the interactions with host rocks and prevalent minerals. Surface adsorption and transformation (including redox and nonredox processes) occurring during the interactions contribute greatly to the immobilization of radionuclides (Chen et al., 2020; Jin et al., 2014; Pan et al., 2017). The adsorption behaviour at the solid-liquid interface is fickle as environmental conditions varying, such as pH, background electrolytes, coexisting ligands, natural organic matters (NOMs) (Fukushi and Fukiage, 2015; P. Li et al., 2017; Tan et al., 2018).

Immobilization of trivalent actinides is critical to environmental protection due to their long half-life and strong radioactivity. Europium(III), i.e., Eu(III), is commonly considered as a chemical analogue for trivalent lanthanides (Ln) and actinides (An) due to the similar electronic and bonding properties (Takahashi et al., 1998a; Bradbury et al., 2002; Stumpf et al., 2002; P. Li et al., 2017; Pan et al., 2017). As such, the retention of Eu(III) on various potential barriers has been extensively investigated to provide fundamental data concerning the performance assessment of HLW repositories and the remediation of radioactive contaminations (Fan et al., 2015;

Fukushi et al., 2013; Jin et al., 2014; Pan et al., 2017; Qiu et al., 2018). It was reported that pH, ionic strength and NOMs largely influenced Eu(III) adsorption on muscovite, bentonite, illite, montmorillonite, granite, soil, etc. (Bradbury and Baeyens, 2009; Fan et al., 2013; Jin et al., 2014; Pan et al., 2017). Previous studies of Eu(III) adsorption on granite showed that Eu-enriched areas of biotite commonly contained less potassium, indicating that ionic exchange was the main process for Eu(III) adsorption on biotite (Fukushi et al., 2013). It has been reported that the influence of cations (mainly alkali and alkaline earth ones) on the ionic exchange process of mica group minerals is not only the competition on adsorption sites but also the steric effects on specific sites (Fan et al., 2014; Tamura et al., 2014). For instance, frayed edge sites (FESs) can be collapsed by cations having smaller hydrated ionic radii (K^+, Cs^+ and NH_4^+), and unavailable interlayer sites can be expanded by cations that have larger hydrated ionic radii (Ca^{2+} and Mg^{2+}). NOMs exist ubiquitously in the aquatic environment, affecting the adsorption of radionuclides mainly through complexing with radionuclides and further enhancing the solubility of radionuclides especially at pH 3-10 (Takahashi et al., 1998a; Tan et al., 2018). The combination of X-ray photoelectron spectroscopy (XPS) and extended X-ray absorption fine structure (EXAFS) approaches indicated that complexation species were different for the different reaction sequences of fulvic acid (FA) and Eu(III) (Fan et al., 2008). More notably, it was confirmed that organic matters could enter and stably stay in the interlayers of expandable clay minerals (Dubbin et al., 2014; Park et al., 2017).

So far, no mature model is available for describing the adsorption of Ln(III)/An(III)

under a wide range of chemical conditions, partially because of the lack of comprehensive study on mica group minerals. For instance, 2:1 phyllosilicate has shown strong decontamination ability, whereas the effects of the various structures and compositions on the adsorption of Eu(III) are rarely investigated on the molecular scale. Mica group minerals, like illite, muscovite, biotite, phlogopite, etc., serving as effective scavengers under either ambient air conditions or the geologic repository environment, always received extensive attention (Mukai et al., 2018; Pan et al., 2017; Wu et al., 2020). This is because mica group minerals are (i) widespread in the environment, (ii) the parent materials of clay minerals (smectite, vermiculite and their mixed-layer mineral, etc.), and (iii) the main components in the host rocks (both granite and clay) that inhibit the migration of radionuclides (Fukushi et al., 2013; H. Li et al., 2019; Wu et al., 2018b). According to the valence of filling ions in the octahedron, micaceous minerals can be divided into dioctahedral and trioctahedral types. The main adsorption sites on dioctahedral mica are planar sites (accounting for ~80% of cation exchange capacity) while its interlayer sites are unavailable (Bradbury and Baeyens, 2000; Fan et al., 2014). On the other hand, the proportion of planar sites on trioctahedral mica (easily weathered) can be down to ~50% with the increase of interlayer sites (the interlayer distance can increase to ~14-20 Å) (Fan et al., 2014; Fan and Takahashi, 2017; Park et al., 2017). The frayed edge site is one kind of specific site on micas that has been confirmed highly selective to Cs^+. Although its fraction is less than ~1%, it is very important for the further availability of interlayer sites (Fan et al., 2014; Wu et al., 2018b; Zachara et al., 2002). The octahedron of mica

is usually a mixture of both dioctahedron and trioctahedron in varying degrees in the environment. Therefore, it is very important to clarify the roles of pure dioctahedral and trioctahedral endmember structures in the process of radionuclides adsorption on mica group minerals.

In this work, dioctahedral muscovite and trioctahedral phlogopite were employed to interact with Eu(III) under various conditions of pH, ionic strength, background electrolyte, and fulvic acid. We expected a better understanding of the adsorption processes of trivalent actinides on micas as well as a critical reference for the predictive model.

2 Materials and methods

2.1 Materials

Muscovite and phlogopite powders (passed through a 325-mesh sieve) used in this work were purchased from the Shikan industrial area of Lingshou County (Hebei Province, China), which have been characterized in detail (Wu et al., 2020). Cation exchange capacities (CECs) of muscovite and phlogopite are 4.01 and 11.15 meq/100 g, respectively. The XRD patterns, formulas and zeta potentials of micas are summarized in Fig. S1. According to the valence and amount of filling cations in octahedrons, muscovite (96.55% trivalent cations) and phlogopite (99.63% divalent cations) can be considered as pure dioctahedral and trioctahedral micas, respectively. The characteristic (001) and (003) diffraction peaks of both muscovite and phlogopite

are at 8^o and 26^o 2-theta, respectively. All chemical reagents of analytical grade were purchased and used without any further purification. All the solutions, including the Eu(III) stock solution that was prepared by dissolving an appropriate amount of $Eu(NO_3)_3 \cdot 6H_2O$ (Aladdin, 99.9%), were made with ultrapure water (18.2 MΩ·cm, Millipore Co.). Salts of NaCl, CsCl and $CaCl_2$ were used to prepare background electrolytes. The FA extracted from natural soil had been characterized previously (Fan et al., 2008).

2.2 Batch adsorption experiments

Batch adsorption experiments with single variable were carried out to compare the adsorption behaviours of Eu(III) onto muscovite and phlogopite. The effects of pH, ionic strength (*I*), background electrolytes, initial Eu(III) concentration, and FA were investigated, and the adsorption behaviours and sequential extraction were used to unravel the adsorption procedures, forms and mechanisms.

All batch experiments were conducted under ambient air conditions. 1.0 g/L muscovite or phlogopite with different background electrolytes in the absence or presence of 50.0 mg/L FA was introduced into 10 mL polyethylene test tubes followed by a pre-equilibrium duration of 24 h without pH adjustment. Afterwards, an appropriate amount of Eu(III) stock solution was added to achieve the target concentrations. The pH values were then adjusted by adding a negligible volume of a HCl and/or NaOH solution (0.1 mol/L). After shaking in an air-bath shaker (BSD-TX270, Shanghai Boxun Medical Biological Instrument Corp.) at 298±1 K for

48 hours, the solid and liquid phases were separated by centrifuging (Thermo Scientific Sorvall ST16R, ThermoFisher scientific) at 10,000 rpm for 10 min. The solid was kept for further characterizations and the supernatant was further filtered by 0.22 μm pore size membrane filters (Polycarbonate, Advantec). The aqueous Eu(III) concentrations after equilibrium (C_e, mol/L) were analyzed by the Inductively Coupled Plasma Optical Emission Spectrometer (ICP-OES, Agilent Technologies 5100) at 420.504 nm wavelength. The concentrations of FA in the supernatant (mg/L) were analyzed at 200 nm by spectrophotometry methods (Dubbin et al., 2014). It has been verified that the presence of FA had an indiscernible effect on Eu(III) determination. Meanwhile, the pH values of the suspensions were measured by a pH electrode (LE422, METTLER TOLEDO). The adsorption percentage (%) of Eu(III) and FA, and the adsorption quantity (Q, mol/g) and the solid-liquid distribution coefficient (K_d, L/g) of Eu(III) were calculated using Eqs. (1)-(3):

$$Adsorption\ (\%) = (C_0 - C_e) / C_0 \times 100\% \quad (1)$$

$$Q = (C_0 - C_e) / (s/l) \quad (2)$$

$$K_d = Q / C_e \quad (3)$$

where C_0 and C_e are the initial Eu(III) or FA concentration (mol/L or mg/L) and the equilibrium concentration in the filtrate (mol/L or mg/L), respectively; s/l (g/L) represents the solid-to-liquid ratio. All the experimental data were the averages of duplicate or triplicate experiments with a relative error of less than 5.0%.

2.3 Sequential extraction

Pre-adsorption experiments of Eu(III) were performed in 50 mL polyethylene test tubes with total volumes of 30.0 mL as exactly described above. In the adsorption systems, the initial Eu(III) concentration was 5.0×10^{-5} mol/L and the pH was maintained at 5.3. Afterwards, the supernatant was isolated to determine the amounts of Eu(III) adsorbed, and the Eu-loaded solid samples were recovered and rinsed rapidly with ultrapure water for the subsequent extraction experiments. The adsorption products were subsequently soaked in solutions of $CaCl_2$ (1.0 mol/L, pH 5.3), NH_4OAc (1.0 mol/L, pH 5.3) and HNO_3 (pH 2). For each extraction procedure, 30.0 mL extraction solution was used; the suspension was continuously shaken for 24 h, then centrifuged and separated. The extraction amount of Eu(III) was calculated from the initial amount of Eu(III) adsorption on muscovite or phlogopite and the amount of Eu(III) in the extraction solutions. Extracted fractions were defined as follows: (i) fraction 1 (F_1) extracted by 1.0 mol/L $CaCl_2$ solution, (ii) faction 2 (F_2) extracted by 1.0 mol/L NH_4OAc solution, (iii) fraction 3 (F_3) dissolved by HNO_3 (pH 2), and (iv) residual fraction (F_4).

2.4 Solid characterization

Characterization was performed on the pristine and Eu-loaded mica powders. The Eu-loaded micas were obtained after adsorption experiments and then freeze-dried under vacuum at -80□ by an FD-1D-80 vacuum freeze dryer (Beijing Boyikang Experiment Instrument Co., Ltd) for 24 h. X-ray diffraction (XRD) patterns of the

192 micas were collected using a powder X-ray diffractometer (X' Pert PRO, Malvern
193 PANalytical) operating at 40 kV and 30 mA with a step interval of 0.02^{o} at a rate of
194 4.0^{o}/min. Transmission electron microscopy (TEM) characterization was performed
195 using a Tecnai G2 F30 (FEI, U.S.) at an operating voltage of 300 kV. The samples for
196 TEM were dispersed sufficiently in ethanol under ultrasonic treatment. After, the
197 obtained homogeneous suspension was dropped onto a copper grid coated with a
198 porous carbon support film, which was dried mildly before the measurement.

199 **3 Results and discussion**

200 **3.1 Effect of pH**

201 Speciation calculations of 5.0×10^{-5} mol/L Eu(III) using PHREEQC (Parkhurst and
202 Appelo, 1999) indicated that Eu^{3+} is the predominant species (more than 80%) below
203 pH 5.7, and aqueous complex with carbonate, hydroxy and/or hydrated ligands prevail
204 at pH >5.7 (Fig. 1A) (Takahashi et al., 1999). Above pH 5.7, ~50% of Eu(III) forms
205 $Eu_2(CO_3)_3\cdot3H_2O$ (aq) in the pH ranges of 5.7-8.8, ~25% and >95% of Eu(III) forms
206 $EuOHCO_3$ (aq) and $Eu(OH)_3$ (aq) in the pH ranges of 8.8-10.3 and 10.3-12.0,
207 respectively. Meanwhile, the saturation indices of $Eu_2(CO_3)_3\cdot3H_2O$, $EuOHCO_3$,
208 $Eu(OH)_3$ are all less than zero (Fig. S2), which indicates that Eu(III) species are all
209 soluble under the conditions. In addition, there are five complexes formed with
210 chloride, hydroxyl, carbonate, and Eu(III) ($EuCl^{2+}$, $Eu_2(OH)_2^{4+}$, $EuOHCO_3$,
211 $EuOH(CO_3)_2^{2-}$ and $Eu(OH)_2CO_3^{-}$), which account for more than 1% at different pH
212 values and is expected to affect considerably the migration behaviour of Eu(III)

213 especially at low Eu(III) concentration (Kyzioł-Komosińska et al., 2019).

214 The adsorption of Eu(III) on muscovite and phlogopite as a function of pH are
215 compared under 0.01 mol/L NaCl background electrolyte (Fig. 1B). At pH <5.0,
216 pH-independent adsorption of Eu(III) on muscovite was observed with around 35%
217 Eu(III) adsorbed constantly, which should be mainly controlled by ionic exchange
218 and/or outer-sphere complexation (Fan et al., 2009; Pan et al., 2017). With increasing
219 pH, the adsorption percentage of Eu(III) (from 35% to 99%) increased quickly in the
220 pH range of 5.0–7.0, and then maintained a high uptake percentage (>99%) above pH
221 7.0. According to the zeta potential of muscovite (Fig. S1B), it decreased sharply in
222 pH ranged from 5.0 to 7.0. Combined with the speciation calculation, Eu(III) mainly
223 forms $Eu_2(OH)_2^{4+}$, $Eu_2(CO_3)_3 \cdot 3H_2O$ (aq), $EuOHCO_3$ (aq) and $Eu(OH)_3$ (aq) above pH
224 5.0 (Fig. 1A). The surface property of muscovite and Eu(III) species supposedly
225 resulted in inner-sphere complexes of Eu(III) formed on mica surface (Takahashi et al.,
226 1998b; Stumpf et al., 2002), which may account for the remarkable increase of
227 adsorption at this pH range. This phenomenon suggests that Eu(III) adsorption on
228 muscovite enhanced the fixation of Eu(III) at pH >5.0, where the strong
229 pH-dependent adsorption under slightly acidic and nearly neutral conditions should be
230 mainly attributed to the adsorption of hydroxyl and/or carbonate surface complexes
231 on muscovite (Sun et al., 2020; Zhou et al., 2020). Note that the surface compositions
232 and properties of adsorbents affect largely the chemical species of Eu(III) during the
233 adsorption process, which may differ from the calculated species in solution. In
234 contrast to muscovite, the pH-dependent adsorption percentage of Eu(III) on

phlogopite increased from 80% at pH 2.0 to 97% at pH >5.0, which is much higher than the case of muscovite. The stronger adsorption on phlogopite can be attributed to the higher CEC and more negative zeta potential (Fig. S1B) than that on muscovite. And the pH-dependent adsorption on phlogopite implied that the adsorption mechanism of Eu(III) was more complex than that of muscovite. Above pH 7.0, the adsorption behaviours of Eu(III) on phlogopite was as similar as muscovite (adsorption percentage >99%). Further confirmation of adsorption forms on muscovite and phlogopite above pH 7.0 was conducted by the XRD results (Fig. S3). It cannot be observed clearly that Eu(III) precipitates generated at pH 8.4. This opinion was also supported by the saturation indices (Fig. S2) and the evidence from Takahashi et al. (1998b) and Stumpf et al. (2002). Although the structures (2:1 phyllosilicates) and compositions (Fig. S1A) of muscovite and phlogopite are relatively close, an obvious difference in Eu(III) adsorption especially below pH 5.0. It is speculated that this phenomenon is due to not only the more negative zeta potential of phlogopite (Fig. S1B) but also the structural difference between dioctahedral and trioctahedral micas.

According to the calculation of CEC, the capacities of muscovite and phlogopite were 4.01×10^{-5} and 1.165×10^{-4} eq/L respectively, which were equal to 26.7% and 77.7% initial Eu(III) concentration (1.5×10^{-4} eq/L). Accordingly, Eu(III) adsorption under acidic conditions was not only controlled by ionic exchange and outer-sphere complexation, but also by inner-sphere complexation, which has been confirmed by laser fluorescence spectroscopy (Takahashi et al., 1998b; Stumpf et al., 2002). Thus,

the effect of high concentration of Eu(III) can be ignored, and the experimental system can be closer to the real environment, which was similar to the systems using radioisotope tracers (Fairhurst et al., 1995; Takahashi et al., 1998a).

3.2 Effect of ionic strength

As shown in Fig. 1B, the ionic strength manifested a significant difference in Eu(III) adsorption between muscovite and phlogopite, where a more obvious effect on muscovite. In the pH range of 2.0-7.0 with increasing ionic strength, the adsorption percentage of Eu(III) by muscovite decreased (i.e., from 0.01 to 0.1 mol/L NaCl), whereas it increased in the case of phlogopite. The result confirmed that ionic exchange and outer-sphere complexation contributed to the Eu(III) adsorption below pH 7.0. At pH >7.0, the effect of ionic strengths led to a negligible difference between muscovite and phlogopite with respect to Eu(III) adsorption (Pan et al., 2017), where the inner-sphere complexation controlled Eu(III) adsorption.

Typically, the higher ionic strength is, the weaker Eu(III) adsorption is when the chemical interactions were controlled by ionic exchange and/or outer-sphere complexation (Fan et al., 2009; Pan et al., 2017). It can be seen that Eu(III) adsorption on muscovite was consistent with that on illite (Bradbury and Baeyens, 2009) and granite (Jin et al., 2014), where weaker adsorption under higher ionic strength resulting from the competition between cations and Eu(III) on the adsorption sites was observed (Zhang et al., 2020; Zhou et al., 2020). Meanwhile, the inhibitory effect of ionic strength on Eu(III) adsorption decreased with the increase in pH. It can be

concluded that Eu(III) adsorption on muscovite was controlled by ionic exchange and/or outer-sphere complexation under acidic conditions while inner-sphere complexation predominated under slightly acidic and neutral conditions (Stumpf et al., 2002; P. Li et al., 2017; Pan et al., 2017). However, the opposite tendency for phlogopite in the pH range of 2.0-7.0 implies different mechanisms. Compared with muscovite, the dissolution of phlogopite released a larger number of cations (e.g., K^+, Mg^{2+}, and Ca^{2+}, etc.). Meanwhile, the densities of dissolved cations are proportional to the solution acidity (Kalinowski and Schweda, 1996). As a result, phlogopite can provide more available sites and more negative electrostatic attraction for Eu(III), indicating that the availability of the sites on trioctahedral mica is higher than that of dioctahedral mica during the adsorption process (Wu et al., 2020). On the other hand, the release of cations (including K^+, Mg^{2+} and Ca^{2+}, etc.) from phlogopite was reduced by a higher Na^+ concentration (Fig. S4), which weakened the competition between cations and Eu(III) and thus enhanced Eu(III) adsorption. Similar observations were reported by previous works (Wu et al., 2020; Yamaguchi et al., 2018).

3.3 Effect of cations

The influence of cations on Eu(III) adsorption by muscovite and phlogopite is shown in Fig. 2. The presence of K^+, Cs^+ and Ca^{2+} inhibited Eu(III) adsorption in different degrees in the pH range of 2.0-7.0 compared with Na^+. For muscovite, the effects of K^+, Cs^+ and Ca^{2+} on Eu(III) adsorption were comparable, where the percentage

299 increased slowly from ~5% at pH 2.0 to ~35% at pH 5.5, sharply to ~99% until pH
300 7.0, and maintained at ~99% at pH >7.0 (Fig. 2A). Considering that the ionic
301 exchange and/or outer-sphere complexation controlled the adsorption in the pH range
302 of 2.0-5.5, it was proved that K^+, Cs^+ and Ca^{2+} are more competitive than Na^+ for
303 Eu(III) adsorption on muscovite. However, ionic exchange on planar sites alone
304 cannot completely explain the experimental data under acidic conditions, which has
305 been supported by the potentiometric and Eu(III) adsorption results on illite (Sinitsyn
306 et al., 2000). The adsorption sites for Cs^+ provided by clay minerals can be divided
307 into four types, of which the planar sites prevail (~80% of the adsorption capacity)
308 and frayed edge sites, edge sites and interlayer sites should not be neglected.
309 (Bradbury and Baeyens, 2000; Fan et al., 2014; Wu et al., 2018b). According to the
310 log *K*, K^+, Cs^+ and Ca^{2+} have stronger affinities towards planar sites of micas
311 compared to Na^+ (Onodera et al., 2017; Park et al., 2017).

312 For phlogopite, results of pH effects showed that Eu(III) adsorption was inhibited
313 following the order of $Cs^+ > K^+ \approx Ca^{2+} > Na^+$(Fig. 2B). In the pH range of 2.0-5.5, the
314 adsorption percentages of Eu(III) in the presence of K^+ and Cs^+ were pH-independent
315 and maintained at ~60% and ~35%, respectively, which showed a similar shape with
316 that on muscovite under 0.01 mol/L Na^+ (Fig. 2A). Combined with previous works
317 (Mukai et al., 2018; Wu et al., 2018a), it can be speculated that the inhibition of Eu(III)
318 adsorption was due to the occupation of frayed edge sites by K^+ and Cs^+, which
319 interrupted the interlayer expansion under acidic conditions. On the other hand, Eu(III)
320 adsorption on phlogopite under Ca^{2+} electrolyte was pH-dependent and increased

stepwise from ~60% to 99% in the pH range of 2.0-7.0 (Fig. 2B). The results supported that the decrease in K^+ and Ca^{2+} concentrations could weaken Eu(III) adsorption on phlogopite under higher ionic strength (0.1 mol/L Na^+) (Fig. 1B).

The different adsorption behaviours of Eu(III) on muscovite and phlogopite can be further interpreted by their XRD patterns at pH 5.3 (Fig. 3). After interacting with Eu(III) under different electrolytes, the main characteristic peaks remained for the muscovite such as (001) and (003) at 8.3^o and 26.2^o 2-theta respectively (Fig. 3A), which were consistent with that of the pristine minerals (Fig. S1A). It suggested that the muscovite structure was almost unchanged. As mentioned above, planar sites contributed mainly to the retention of Eu(III) by muscovite whereas it was not the case for phlogopite. As reported previously, the interlayer K^+ of phlogopite tended to be replaced by cations with larger ionic potentials or smaller hydrated ionic radii, leading to an interlayer expansion or collapse (Tamura et al., 2014). The XRD patterns of phlogopite (Fig. 3B) can be classified into two kinds: one is consistent with the pristine phlogopite (Fig. S1A) under K^+ and Cs^+ electrolytes, the other shows new features at 6^o 2-theta under Na^+ and Ca^{2+} electrolytes. Without the interlayer expansion, Eu(III) adsorption on phlogopite under K^+ and Cs^+ electrolytes confirmed the main contribution from planar sites. Considering no obvious difference in XRD patterns was observed after contacting with Cs^+ and K^+ electrolyte, the ~30% gap for Eu(III) adsorption on phlogopite (Fig. 2B) demonstrates that Cs^+ is more competitive than K^+ on planar sites of phlogopite (Bradbury and Baeyens, 2000; Fan et al., 2014). Moreover, the same proportion of pH-independent Eu(III) adsorption was kept

between phlogopite under 0.01 mol/L Cs^+ and muscovite under 0.01 mol/L Na^+, which indicates the important contribution of interlayer sites and planar sites of phlogopite. On the contrary, a new (001) diffraction peak at 6^o 2-theta (indicating an interlayer distance of 15 Å) caused by Eu(III) adsorption suggested that the interlayer sites of phlogopite largely contributed to Eu(III) retention (Kyzioł-Komosińska et al., 2019). Compared to Na^+, the stronger diffraction peak at 6^o 2-theta in the case of Ca^{2+} (Fig. 3B) should result from the stronger competition ability of divalent Ca^{2+} towards the interlayer sites of phlogopite. As illustrated in Fig. 2B, the percentage of Eu(III) adsorption with Ca^{2+} is smaller than the Na^+ case at pH 5.3, confirming that the strong adsorption competition between Ca^{2+} and Eu^{3+} should be responsible for the interlayer expansion of phlogopite. Moreover, the pH-dependent expansions have been also observed during the adsorption of Th(IV) and Sr(II) on phlogopite (Wu et al., 2020; 2018a).

The selected area electron diffraction (SAED) patterns and the TEM images of Eu(III)-loaded muscovite and phlogopite were shown in Fig. 4. The typical hexagonal structure of muscovite after Eu(III) adsorption (Fig. 4A) was confirmed by the SAED pattern (Yu et al., 2006), demonstrating that Eu(III) adsorption did not change the structure of muscovite. In contrast, the layers on the edge of phlogopite powder were thinner than the central part after adsorbing Eu(III) (Fig. 4B). Besides, the corresponding diffraction rings (Fig. 4C) and ordered diffraction spots (Fig. 4D) confirmed that the crystallinity degree of phlogopite, especially of its layer edge, was decreasing (L. Wang et al., 2016). This is in good agreement with its weakly diffuse

XRD peaks and the appearance of new diffraction at 6^{o} 2-theta (Fig. S5), suggesting that phlogopite vermiculized during Eu(III) adsorption (L. Wang et al., 2016). Therefore, the synergistic adsorption and structural alteration could play key roles in the retardation of radionuclides on trioctahedral micas rather than dioctahedral ones under real environmental conditions.

3.4 Effects of Eu(III) concentration

The concentration of Eu(III) is often a key factor affecting the adsorption behaviour. Considering that no significant difference was observed in the XRD patterns of muscovite samples in Fig. 3B, this section mainly focuses on the structural change of phlogopite potentially related to the initial Eu(III) concentration. At pH 5.3, the values of K_d at different initial concentrations of Eu(III) on phlogopite were 4.3, 29.9 and 180.8 L/g, respectively (Fig. S5A). The corresponding XRD patterns are shown in Fig. S5B, illustrating that the larger the K_d is, the higher the relative intensity of the diffraction peak at 6^{o} 2-theta is. Nevertheless, the K_d value is determined not only by the interlayer sites that can be reflected by the position and intensity of the diffraction peaks along the (001) direction, but also by the large contribution of the planar sites. Since the contributions from the two types of sites are hard to be separated, the quantitative relation between the relative intensity of diffraction peak at 2-theta 6^{o} and the capacity of interlayer sites cannot be established directly.

As discussed above, the addition of Cs^{+} could hinder significantly the interaction between Eu(III) and phlogopite. Thus, it is critical to investigate the effect of the

addition order of Cs^+ and Eu(III) on the adsorption capacity and the structural alteration of phlogopite. Fig. 5A shows the effect of the reaction sequence on the interaction between Eu(III) and phlogopite. Three typical cases were investigated: (i) adding Cs^+ after Eu(III) interacting with phlogopite for 24 h and then reacting together for 24 h; (ii) adding Eu(III) and Cs^+ together into the phlogopite suspension and reacting for 48 h; (iii) adding Eu(III) after Cs^+ equilibrating with phlogopite for 24 h and then reacting together for 48 h. Accordingly, all the three adsorption behaviours of Eu(III) at pH 2.0-7.0 showed different shapes: (i) Eu(III) adsorption increases from ~45% at pH 2.0 to ~97% at pH 7.0, which is similar to that of phlogopite under Na^+ background (Fig. 1B); (ii) the adsorption of Eu(III) on phlogopite under Cs^+ background, as discussed above, is nearly the same with that of muscovite under Na^+ background (Fig. 2A); (iii) the percentage of Eu(III) adsorption firstly increases from ~5% at pH 2.0 to ~40% at pH 4.0 and maintains at ~40% in the pH range of 4.0-6.0, and then rises steeply to ~97% at pH 7.0.

It can be seen that the pre-equilibrium of phlogopite with Cs^+ led to a very low adsorption percentage of Eu(III) at pH < 4.0. Cs^+ can prevent the interlayer expansion, occupy the effective sites of phlogopite, and weaken the electrostatic attraction of phlogopite to Eu^{3+} (Fan et al., 2014; Mukai et al., 2018). Subsequently, Eu(III) adsorption at pH 4.0-7.0 shows that the competitiveness of Eu(III) on the available sites of phlogopite becomes stronger with increasing pH. Previous works on Th(IV) (less than 5.0×10^{-5} mol/L) also showed a strong affinity towards phlogopite via occupying the interlayer sites (Fan et al., 2014; Wu et al., 2020; 2018a). Likewise, this

process can be inhibited by Cs^+ through collapsing frayed edge sites of phlogopite (Fan et al., 2014; Wu et al., 2020; 2018a).

In addition to the reaction sequence, the concentration ratio of Eu(III) to Cs^+ (Eu/Cs ratio) also affects the structure of phlogopite. Fig. 5B shows the XRD patterns of phlogopite after Eu(III) adsorption under Cs^+ background with two different Eu/Cs ratios. At Eu/Cs ratio of 100 (1.0×10^{-4} mol/L Eu(III) to 1.0×10^{-6} mol/L Cs^+) the relative intensity of the diffraction peak at 6^o 2-theta is nearly 100%. Whereas, this diffraction peak is almost invisible with an Eu/Cs ratio of 0.005 (5.0×10^{-5} mol/L Eu(III) to 0.01 mol/L Cs^+), indicating that the interlayer of phlogopite was not enlarged. It is commonly known that the capacity of frayed edge sites is ~10^{-7} mol/g (Bradbury and Baeyens, 2000; Fan et al., 2014), thus Cs^+ with a higher concentration than the site capacity can collapse the frayed edge sites. In this work, we found that the interlayer sites could be also affected and expanded significantly at high Eu/Cs ratios.

3.5 Effects of FA

The effect of FA (one of the common NOMs) is also a key factor that is worth investigating thoroughly (Stockdale and Bryan, 2013; Tan et al., 2018; Zhang et al., 2020). The purification and preparation of the natural FA in this work have been described in detail in previous work (Fan et al., 2008), and the major element composition (mass%) is C (50.15), H (4.42), N (5.38), O (39.56) and S (0.49). The effects of FA on Eu(III) adsorption under different background electrolytes are shown

429 in Figs. 6A (muscovite) and 6B (phlogopite). In the presence of FA, the adsorption of
430 Eu(III) on muscovite (Fig. 6A) was suppressed (especially above pH 6.0) and showed
431 a similar trend under both Na^+ and Cs^+ background from pH 2.0 to 11.0. It gradually
432 increased from ~5% at pH 2.0 to ~60% at pH 6.5, and then decreased gradually to less
433 than 5% at pH 11.0 (Fairhurst et al., 1995; Takahashi et al., 1999; X. Wang et al.,
434 2016). An opposite phenomenon occurred on phlogopite below pH 6.5, that is Eu(III)
435 adsorption was enhanced by FA (Fig. 6B) characterized with a sharp increase under
436 Cs^+ background and a slight increase under Na^+ background. Above pH 6.5, Eu(III)
437 adsorption under both Na^+ and Cs^+ electrolytes decreased in the presence of FA (a
438 subsequent decrease from ~98% at pH 6.5 to ~40% at pH 11.0). Generally, NOMs and
439 lanthanide ions have strong binding abilities and form thermodynamically stable
440 species via sharing oxygen atoms (Takahashi et al., 1999; Tan et al., 2018), i.e.
441 Ln-NOMs hybrids. The strong complexation strength in soluble Eu-FA hybrids results
442 in significant changes in the adsorption behaviours of Eu(III).

443 The adsorption behaviours of FA on muscovite and phlogopite (Fig. 6C) are expected
444 to provide more clues for understanding the effect of FA on Eu(III) adsorption and the
445 relevant mechanisms. FA showed a stronger affinity towards phlogopite compared
446 with muscovite. With increasing pH, the removal percentage of FA on phlogopite
447 increased slowly from ~90% to ~95% while that on muscovite maintained around 60%
448 followed by an obvious decrease to ~40% at pH above 10.0. As can be seen, the
449 stronger adsorption capacity of phlogopite compared to muscovite, which is
450 determined by the differences in surface charges and functional groups of the

451 dioctahedral and trioctahedral micas (Kitayama et al., 2020), is also effective for FA.
452 In the ternary systems, the adsorption percentage of FA gradually decreased from ~60%
453 (for muscovite) and ~90% (for phlogopite) at pH 2.0 to ~5% at pH 11.0. The
454 enhancement of Eu(III) adsorption on phlogopite below pH 6.5 can be explained by
455 taking into account the high proportion of FA adsorbed to the mica surface (Fig. 6C)
456 in the presence of Eu(III). Combined with inhibition by FA on Eu(III) adsorption on
457 both muscovite and phlogopite under alkaline conditions (Figs. 6A and 6B), it
458 suggested that soluble Eu-FA hybrids preferred retaining in the liquid phase (Fairhurst
459 et al., 1995; Takahashi et al., 1998a and 1999; Z. Li et al., 2019; Tan et al., 2018),
460 especially in the case of muscovite.

461 Remarkably, although FA reduced Eu(III) adsorption on both micas under alkaline
462 conditions, under acidic conditions it enhanced the Eu(III) adsorption on phlogopite
463 but inhibited that on muscovite. Besides, the enhancement effect of FA in the case of
464 phlogopite was more apparent under Cs^+ electrolyte (Fig. 6B). Previous work reported
465 that NOMs could hinder the adsorption of Cs^+ on frayed edge sites, thus further
466 reduce the availability of interlayer sites (Fan et al., 2014). XRD patterns in Fig. 6D
467 suggested that Eu(III) adsorption on phlogopite that was pre-equilibrated with the FA
468 would not induce interlayer expansion (0.01 mol/L Na^+, at pH 5.3). On the contrary,
469 the interlayer expansion of phlogopite occurred when Eu(III) was introduced prior to
470 the FA. The relative intensity of diffraction peak at 6^o 2-theta is stronger than that in
471 the absence of FA (Fig. 3B). This phenomenon implies that FA might facilitate the
472 interlayer expansion of phlogopite after Eu(III) occupied the interlayer sites, whereas

it may block the access and restrain the further expansion of phlogopite before adding Eu(III) (Dubbin et al., 2014; Wu et al., 2018a). Therefore, the enhancement of Eu(III) adsorption by FA when using Cs^+ as the background was mainly attributed to the formation of Eu-FA hybrids on the planar sites of phlogopite (Fan et al., 2009; X. Wang et al., 2016). These results confirmed that NOMs can significantly influence the mobility and bioavailability of Eu(III), and also the interlayer expansion of trioctahedral micas.

3.6 Sequential extraction

Sequential extraction was performed to identify the adsorption forms of Eu(III) on muscovite and phlogopite based on the well-developed method (Martin et al., 1998; Rauret et al., 1999). As shown in Fig. 7, the results of Eu(III) extracted yield (%) from Eu-loaded muscovite and phlogopite under different background electrolytes (Na^+ and Cs^+) in the absence or presence of FA were compared. By calculation, the percentages of residual fraction (F_4) are less than 5%, suggesting that almost all the adsorbed Eu(III) was extracted by three-step sequential experiments. Regents of Ca^{2+} and NH_4^+ were used to extract the adsorbed Eu(III) species of the ionic exchange forms and/or outer-sphere complexation, while HNO_3 (pH 2) was employed to dissolve the inner-sphere complexes and/or surface precipitate of Eu(III) (Martin et al., 1998; Rauret et al., 1999). Fig. 7A showed that more than 90% of Eu(III) on muscovite under Na^+ electrolyte was in the exchangeable form, whereas it decreased to ~80% and ~50% in the presence of Cs^+ and FA, respectively. For phlogopite, ~80% of Eu(III)

494 was in the exchangeable form under both electrolytes of Na^+ and Cs^+ (Fig. 7B),
495 suggesting that phlogopite had a stronger affinity towards Eu(III) than muscovite.
496 Meanwhile, F_3 accounted for 4%-20% under Na^+ and Cs^+ electrolytes supported the
497 view of adsorption mechanism below pH 6.5, that is inner-sphere complexation
498 participated in Eu(III) adsorption. In addition, the presence of FA increased the
499 percentage of inner-sphere Eu(III) complexes to ~40%, which was slightly higher
500 than that on muscovite. It can be concluded that the mobility of Eu(III) was largely
501 controlled by the structure configurations of micas, background electrolytes and
502 NOMs. It can be concluded that trioctahedral phlogopite is an effective adsorbent to
503 inhibit the migration and bioavailability of Eu(III), especially in the presence of FA in
504 the pH range of 2.0-7.0.

505 **4 Conclusions**

506 This work mainly investigated the adsorption and mechanism of Eu(III) on
507 dioctahedral muscovite and trioctahedral phlogopite under weakly acidic conditions,
508 in the terms of the corresponding alteration in mica structures and the influence of
509 background electrolytes, interaction sequence and FA. The adsorption quantity of
510 Eu(III) on micas ranged from 8.83×10^{-10} to 4.9×10^{-8} mol/kg, where the result of trace
511 concentration was significant to the real environment. Results showed that
512 trioctahedral phlogopite provided superior adsorption capacity for Eu(III) than
513 dioctahedral muscovite, especially at pH 2.0-7.0 (from ~80% to ~97% adsorption).
514 Limited by the fixed amount of planar sites and the unavailable interlayer sites,

dioctahedral muscovite showed a quite weak affinity towards Eu(III) and resulted in ~30% removal in the pH range of 2.0-5.0. The Eu(III) adsorption on dioctahedral muscovite was strongly pH-dependent but weakly dependent on ionic strength (Na^+), while on trioctahedral phlogopite it was nearly independent on both pH and ionic strength (Na^+). High ionic strength (Na^+) enhanced Eu(III) adsorption on phlogopite slightly, which supported the inhibition of adsorption by other cations (Ca^{2+}, K^+ and Cs^+). The XRD analysis also verified that Eu(III) can intercalate into the interlayer of phlogopite under Na^+ and Ca^{2+} background electrolytes, whereas it cannot lead to the interlayer expansion under K^+ and Cs^+ backgrounds but the collapse of the frayed edge sites. The comparison among SAED patterns of micas further confirmed that Eu(III) adsorption occurred on the planar sites of muscovite and both planar sites and interlayer sites of phlogopite. Moreover, the expansion extent of phlogopite interlayer was positively correlated to the K_d of Eu(III) under 0.01 mol/L NaCl; 180.8 L/g Eu(III)-loaded phlogopite resulted in the maximum relative intensity of the diffraction peak (at 6^o 2-theta) corresponding to the enlarged interlayer spacing. Eu/Cs ratio is also a key factor to control the interlayer expansion of phlogopite. The relative intensities of XRD peaks of the expanded interlayers were found to be nearly 100% and 0% at Eu/Cs ratios of 100 and 0.005, respectively. Apart from the electrolyte cations and Eu(III) concentrations, FA can influence Eu(III) adsorption and the expansion of trioctahedral phlogopite simultaneously. The soluble Eu-FA hybrids are expected to be more stable than the surface complexes of Eu(III) under alkaline conditions. The subsequent addition of the FA into the pre-equilibrated system of

Eu(III) and phlogopite enhanced the interlayer expansion, suggesting that NOMs were able to occupy interlayer sites of trioctahedral mica. The pseudocolloid composed of Eu(III) and FA is expected to be immobilization only by trioctahedral phlogopite below pH 6.0 in the environment. The comprehensive and systematic study on Eu(III) adsorption at micas/water interfaces addressed currently could provide important insights into a reliable prediction of Ln/An(III) migration behaviours in dioctahedral or trioctahedral mica-rich environments.

Acknowledgments

This work was supported by the National Natural Science Foundation of China [grant numbers 21906187 and 41773095]; and the Fundamental Research Funds for the Central Universities [grant number 45000-31610037 and 45000-18833403].

548 **Reference**

549 Bradbury, M.H., Baeyens, B., 2009. Sorption modelling on illite Part I: Titration
550 measurements and the sorption of Ni, Co, Eu and Sn. Geochim. Cosmochim. Ac.
551 73, 990–1003. doi:10.1016/j.gca.2008.11.017
552 Bradbury, M. H., Baeyens, B., 2002. Sorption of Eu on Na-and Ca-montmorillonites:
553 experimental investigations and modelling with cation exchange and surface
554 complexation. Geochim. Cosmochim. Ac. 66, 2325-2334.
555 doi:10.1016/S0016-7037(02)00841-4
556 Bradbury, M.H., Baeyens, B., 2000. A generalised sorption model for the
557 concentration dependent uptake of caesium by argillaceous rocks. J. Contam.
558 Hydrol. 42, 141–163. doi:10.1016/s0169-7722(99)00094-7
559 Chen, P., Ma, Y., Kang, M., Shang, C., Song, Y., Xu, F., Wang, J., Song, G., Yang,
560 Y., 2020. The redox behavior of uranium on Beishan granite: Effect of Fe^{2+} and
561 Fe^{3+} content. J. Environ. Radioactiv. 217, 106208.
562 doi:10.1016/j.jenvrad.2020.106208
563 Dubbin, W.E., Vetterlein, J.P., Jonsson, J.L., 2014. Fatty acids promote fulvic acid
564 intercalation by montmorillonite. Appl. Clay Sci. 97-98, 53–61.
565 doi:10.1016/j.clay.2014.05.022
566 Fairhurst, A. J., Warwick, P., Richardson, S., 1995. The effect of pH on
567 europium-mineral interactions in the presence of humic acid. Radiochim. Acta. 69,
568 103-111. doi:10.1524/ract.1995.69.2.103
569 Fan, Q., Li, P., Zheng, Z., Wu, W., Liu, C., 2013. Insights into sorption species of

570 Eu(III) on γ-Al_2O_3 and bentonite under different pH: Studies at macro- and
571 micro-scales. J. Radioanal. Nucl. Ch. 299, 1767–1775.
572 doi:10.1007/s10967-013-2819-x
573 Fan, Q., Takahashi, Y., 2017. Employment of the generalized adsorption model for
574 the prediction of the solid-water distribution of radiocesium in the
575 river-estuary-ocean system. Appl. Geochem. 79, 75–84.
576 doi:10.1016/j.apgeochem.2017.01.020
577 Fan, Q., Tan, X.L., Li, J.X., Wang, X.K., Wu, W., Montavon, G., 2009. Sorption of
578 Eu(III) on Attapulgite Studied by Batch, XPS, and EXAFS Techniques. Environ.
579 Sci. Technol. 43, 5776–5782. doi:10.1021/es901241f
580 Fan, Q., Tanaka, M., Tanaka, K., Sakaguchi, A., Takahashi, Y., 2014. An EXAFS
581 study on the effects of natural organic matter and the expandability of clay
582 minerals on cesium adsorption and mobility. Geochim. Cosmochim. Ac. 135, 49–
583 65. doi:10.1016/j.gca.2014.02.049
584 Fan, Q., Zhao, X.L., Ma, X.X., Yang, Y.B., Wu, W., Zheng, G.D., Wang, D.L., 2015.
585 Comparative adsorption of Eu(III) and Am(III) on TPD. Environ Sci-Proc Imp 17,
586 1634–1640. doi:10.1039/c5em00240k
587 Fan, Wu, W., Song, X.P., Xu, J.Z., Hu, J., Niu, Z.W., 2008. Effect of humic acid,
588 fulvic acid, pH and temperature on the sorption-desorption of Th(IV) on
589 attapulgite. Radiochim. Acta. 96, 159–165. doi:10.1524/ract.2008.1475
590 Fukushi, K., Fukiage, T., 2015. Prediction of Intrinsic Cesium Desorption from
591 Na-Smectite in Mixed Cation Solutions. Environ. Sci. Technol. 49, 10398–10405.

592 doi:10.1021/acs.est.5b01884

593 Fukushi, K., Hasegawa, Y., Maeda, K., Aoi, Y., Tamura, A., Arai, S., Yamamoto, Y.,
594 Aosai, D., Mizuno, T., 2013. Sorption of Eu(III) on granite: EPMA, LA-ICP-MS,
595 batch and modeling studies. Environ. Sci. Technol. 47, 12811–12818.
596 doi:10.1021/es402676n

597 Jin, Q., Wang, G., Ge, M., Chen, Z., Wu, W., Guo, Z., 2014. The adsorption of Eu(III)
598 and Am(III) on Beishan granite: XPS, EPMA, batch and modeling study. Appl.
599 Geochem. 47, 17–24. doi:10.1016/j.apgeochem.2014.05.004

600 Kalinowski, B.E., Schweda, P., 1996. Kinetics of muscovite, phlogopite, and biotite
601 dissolution and alteration at pH 1–4, room temperature. Geochim. Cosmochim.
602 Ac. 60, 367–385. doi:10.1016/0016-7037(95)00411-4

603 Kitayama, R., Yanai, J., Nakao, A., 2020. Ability of micaceous minerals to adsorb
604 and desorb caesium ions: Effects of mineral type and degree of weathering. Eur. J.
605 Soil. Sci. 71, 641–653. doi:10.1111/ejss.12913

606 Kyzioł-Komosińska, J., Janeczek, J., Krzykawski, T., Fabiańska, M.J., Matuszewska,
607 A., Dzieniszewska, A., Teper, E., Pająk, M., Sawicka, N., 2019. Adsorption of
608 Eu(III) onto bentonite and phyllite: A comparative study. Appl. Clay Sci. 183,
609 105330. doi:10.1016/j.clay.2019.105330

610 Li, H., He, B., Li, P., Fan, Q., Wu, H., Liang, J., Liu, C., Yu, T., 2019. Adsorption
611 behaviors of Eu(III) on granite: batch, electron probe micro-analysis and
612 modeling studies. Environ Earth Sci 78, 989. doi:10.1007/s12665-019-8170-y

613 Li, P., Wu, H., Liang, J., Yin, Z., Pan, D., Fan, Q., Xu, D., Wu, W., 2017. Sorption of

614 Eu(III) at feldspar/water interface: effects of pH, organic matter, counter ions, and
615 temperature. Radiochim. Acta. 105, 1049–1058. doi:10.1515/ract-2017-2797
616 Li, Z., Hadioui, M., Wilkinson, K.J., 2019. Conditions affecting the release of thorium
617 and uranium from the tailings of a niobium mine. Environ. Pollut. 247, 206–215.
618 doi:10.1016/j.envpol.2018.12.042
619 Ma, Y., Cheng, X., Kang, M., Yang, G., Yin, M., Wang, J., Gang, S., 2020. Factors
620 influencing the reduction of U(VI) by magnetite. Chemosphere 254, 126855–.
621 doi:10.1016/j.chemosphere.2020.126855
622 Martin, R., Sanchez, D.M., Gutierrez, A.M., 1998. Sequential extraction of U, Th, Ce,
623 La and some heavy metals in sediments from Ortigas river, Spain. Talanta. 46,
624 1115–1121. doi:10.1016/S0039-9140(97)00374-3
625 Mukai, H., Tamura, K., Kikuchi, R., Takahashi, Y., Yaita, T., Kogure, T., 2018.
626 Cesium desorption behavior of weathered biotite in Fukushima considering the
627 actual radioactive contamination level of soils. J. Environ. Radioactiv. 190-191,
628 81–88. doi:10.1016/j.jenvrad.2018.05.006
629 Niu, Z., Fan, Q., Wang, W., Xu, J., Chen, L., Wu, W., 2009. Effect of pH, ionic
630 strength and humic acid on the sorption of uranium(VI) to attapulgite. Appl
631 Radiat Isot 67, 1582–1590. doi:10.1016/j.apradiso.2009.03.113
632 Onodera, M., Kirishima, A., Nagao, S., Takamiya, K., Ohtsuki, T., Akiyama, D., Sato,
633 N., 2017. Desorption of radioactive cesium by seawater from the suspended
634 particles in river water. Chemosphere 1–46.
635 doi:10.1016/j.chemosphere.2017.07.078

636 Pan, D., Fan, F., Wang, Y., Li, P., Hu, P., Fan, Q., Wu, W., 2017. Retention of Eu(III)
637 in muscovite environment: Batch and spectroscopic studies. Chem. Eng. J. 330,
638 559–565. doi:10.1016/j.cej.2017.07.184
639 Park, C.W., Kim, B.H., Yang, H.-M., Seo, B.-K., Moon, J.-K., Lee, K.-W., 2017.
640 Removal of cesium ions from clays by cationic surfactant intercalation.
641 Chemosphere 168, 1068–1074. doi:10.1016/j.chemosphere.2016.10.102
642 Parkhurst, D.L., Appelo, C.A.J., 1999. User's guide to PHREEQC (Version 2): A
643 computer program for speciation, batch-reaction, one-dimensional transport, and
644 inverse geochemical calculations. doi:10.3133/wri994259
645 Qiu, L., Scott, K., Rousseau, S., 2018. Kinetic and equilibrium studies of Cs(I), Sr(II)
646 and Eu(III) adsorption on a natural sandy soil. Radiochim. Acta. 107, 55–66.
647 doi:10.1515/ract-2018-2976
648 Rauret, G., Lopez-Sanchez, J.F., Sahuquillo, A., Rubio, R., Davidson, C., Ure, A.,
649 Quevauviller, P., 1999. Improvement of the BCR three step sequential extraction
650 procedure prior to the certification of new sediment and soil reference materials. J.
651 Environ. Monitor. 1, 57–61. doi:10.1039/A807854H
652 Sinitsyn, V. A., Aja, S. U., Kulik, D. A., Wood, S. A., 2000. Acid−base surface
653 chemistry and sorption of some lanthanides on K^+-saturated Marblehead illite: I.
654 Results of an experimental investigation. Geochim. Cosmochim. Ac. 64, 185-194.
655 doi:10.1016/S0016-7037(99)00175-1
656 Stockdale, A., Bryan, N.D., 2013. The influence of natural organic matter on
657 radionuclide mobility under conditions relevant to cementitious disposal of

radioactive wastes: A review of direct evidence. Earth Science Reviews 121, 1–17. doi:10.1016/j.earscirev.2013.02.007

Stumpf, T., Bauer, A., Coppin, F., Fanghänel, T., Kim, J. I., 2002. Inner-sphere, outersphere and ternary surface complexes: a TRLFS study of the sorption process of Eu (III) onto smectite and kaolinite. Radiochim. Acta. 90, 345-349. doi:10.1007/BF02389785

Sun, Z., Chen, Y.-G., Cui, Y.-J., Ye, W.-M., 2020. Adsorption of Eu(III) onto Gaomiaozi bentonite corroded by cement waters: Effect of cement solutions on the long-term sorption performance of bentonite in the repository conditions. Journal of Cleaner Production 251, 119692. doi:10.1016/j.jclepro.2019.119692

Takahashi, Y., Minai, Y., Kimura, T., Tominaga, T., 1998a. Adsorption of europium(III) and americium(III) on kaolinite and montmorillonite in the presence of humic acid. J. Radioanal. Nucl. Chem. 234, 277-282. doi:10.1007/BF02389785

Takahashi, Y., Kimura, T., Kato, Y., Minai, Y., Tominaga, T., 1998b. Characterization of Eu(III) species sorbed on silica and montmorillonite by laser-induced fluorescence spectroscopy. Radiochim. Acta. 82, 227-232. doi:10.1524/ract.1998.82.special-issue.227

Takahashi, Y., Minai, Y., Ambe, S., Makide, Y., Ambe, F., 1999. Comparison of adsorption behavior of multiple inorganic ions on kaolinite and silica in the presence of humic acid using the multitracer technique. Geochim. Cosmochim. Ac. 63, 815-836. doi:10.1016/S0016-7037(99)00065-4

Tamura, K., Kogure, T., Watanabe, Y., Nagai, C., Yamada, H., 2014. Uptake of cesium and strontium ions by artificially altered phlogopite. Environ. Sci. Technol. 48, 5808–5815. doi:10.1021/es4052654

Tan, L., Tan, X., Mei, H., Ai, Y., Sun, L., Zhao, G., Hayat, T., Alsaedi, A., Chen, C., Wang, X., 2018. Coagulation behavior of humic acid in aqueous solutions containing Cs^{+}, Sr^{2+} and Eu^{3+}: DLS, EEM and MD simulations. Environ. Pollut. 236, 835–843. doi:10.1016/j.envpol.2018.02.019

Wang, L., Wang, X., Yin, J., Wang, C., 2016. Insights into the physicochemical characteristics from vermiculite to silica nanosheets. Appl. Clay Sci. 132-133, 17–23. doi:10.1016/j.clay.2016.05.006

Wang, X., Yu, S., Chen, Z., Song, W., Chen, Y., Hayat, T., Alsaedi, A., Guo, W., Hu, J., Wang, X., 2016. Complexation of radionuclide $^{152+154}$Eu(III) with alumina-bound fulvic acid studied by batch and time-resolved laser fluorescence spectroscopy. Sci. China Chem. 60, 107–114. doi:10.1007/s11426-016-0163-6

Wu, H., Lin, S., Cheng, X., Chen, J., Ji, Y., Xu, D., Kang, M., 2020. Comparative study of strontium adsorption on muscovite, biotite and phlogopite. J. Environ. Radioactiv. 225, 106446. doi:10.1016/j.jenvrad.2020.106446

Wu, H., Qiang, S., Fan, Q., Zhao, X., Liu, P., Li, P., Liang, J., Wu, W., 2018a. Exploring the relationship between Th(IV) adsorption and the structure alteration of phlogopite. Appl. Clay Sci. 152, 295–302. doi:10.1016/j.clay.2017.11.026

Wu, H., Zhao, X., Wang, W., He, B., Geng, R., Fan, Q., 2018b. Interaction mechanism of radioactive cesium on Beishan granite. Sci Sin Chim 49, 165–174.

doi:10.1360/N032018-00146

Yamaguchi, A., Tanaka, M., Kurihara, Y., Takahashi, Y., 2018. Local structure of strontium adsorbed on 2:1 clay minerals and its comparison with cesium by XAFS in terms of migration of their radioisotopes in the environment. J. Radioanal. Nucl. Ch. 1–7. doi:10.1007/s10967-018-5895-0

Yu, X., Zhao, L., Gao, X., Zhang, X., Wu, N., 2006. The intercalation of cetyltrimethylammonium cations into muscovite by a two-step process: I. The ion exchange of the interlayer cations in muscovite with Li. Journal of Solid State Chemistry 179, 1569–1574. doi:10.1016/j.jssc.2006.02.009

Zachara, J.M., Smith, S.C., Liu, C., McKinley, J.P., Serne, R.J., Gassman, P.L., 2002. Sorption of Cs^+ to micaceous subsurface sediments from the Hanford site, USA. Geochim. Cosmochim. Ac. 66, 193–211. doi:10.1016/S0016-7037(01)00759-1

Zhang, H., He, H., Liu, J., Li, H., Zhao, S., Jia, M., Yang, J., Liu, N., Yang, Y., Liao, J., 2020. Sorption behavior of Eu(□) on Tamusu clay under strong ionic strength: Batch experiments and BSE/EDS analysis. Nuclear Engineering and Technology. doi:10.1016/j.net.2020.06.009

Zhou, W., Shi, Y., Li, Y., Xian, D., Wang, J., Liu, C., 2020. Adsorption of Eu(III) at rutile/water interface: Batch, spectroscopic and modelling studies. Colloid. Surface. A 125811. doi:10.1016/j.colsurfa.2020.125811

721 **Figures**

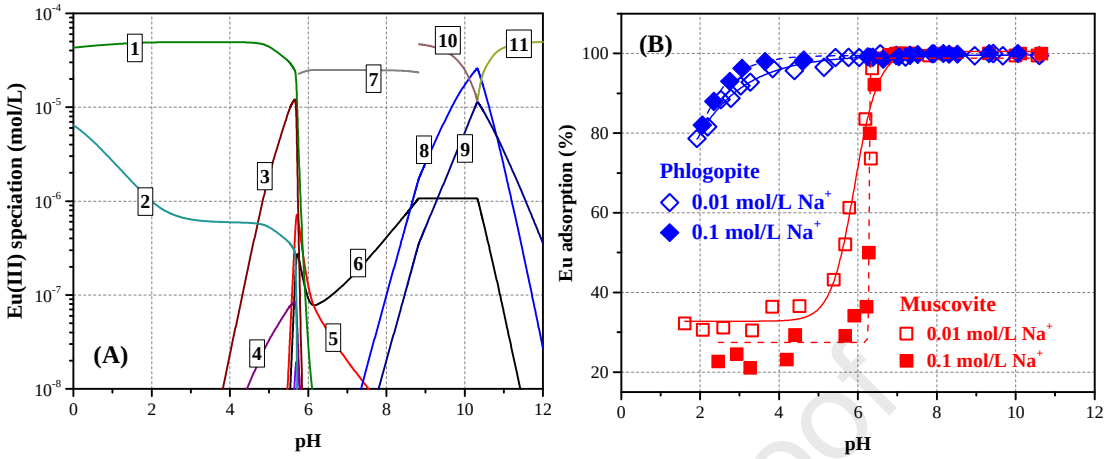

722

723 Fig. 1. (A) The dominant species of 5.0×10^{-5} mol/L Eu(III) calculated by PHREEQC,

724 1-Eu^{3+}, 2-$EuCl^{2+}$, 3-$Eu_2(OH)_2^{4+}$, 4-$EuOH^{2+}$, 5-$EuCO_3^{+}$, 6-$EuOHCO_3$,

725 7-$Eu_2(CO_3)_3\cdot3H_2O$ (aq), 8-$EuOH(CO_3)_2^{2-}$, 9-$Eu(OH)_2CO_3^{-}$, 10-$EuOHCO_3$ (aq),

726 11-$Eu(OH)_3$ (aq) (T = 298±1 K, I = 0.01 mol/L NaCl, $P(CO_2)$ = $10^{-3.42}$ atm) and (B)

727 Effects of pH and ionic strength on Eu(III) adsorption by muscovite and phlogopite (T

728 = 25±1 □, s/l = 1.0 g/L, $[Eu(III)]_{initial}$ = 5.0×10^{-5} mol/L, 48 h).

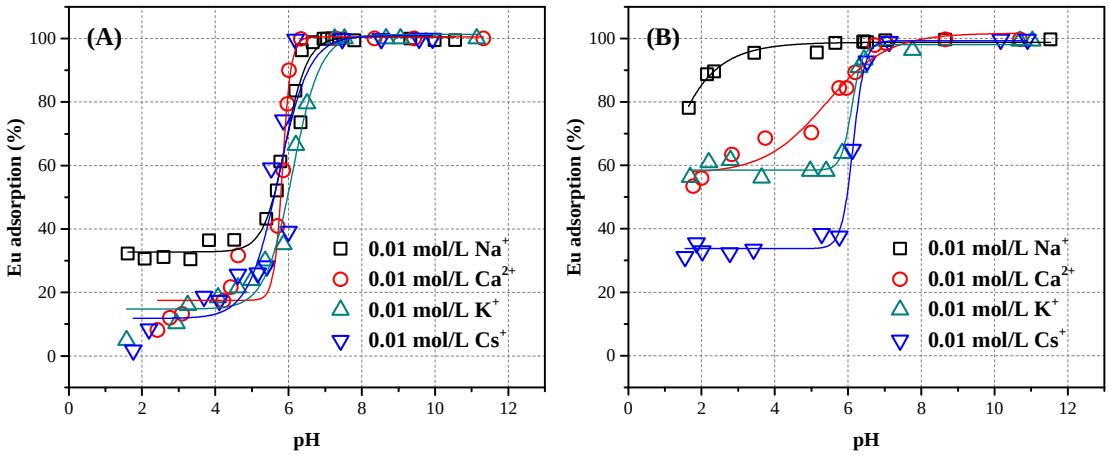

729

730 Fig. 2. Effect of the background electrolyte on Eu(III) adsorption by (A) muscovite

731 and (B) phlogopite (T = 25±1 □, s/l = 1.0 g/L, $[Eu(III)]_{initial}$ = 5.0×10^{-5} mol/L, 48 h).

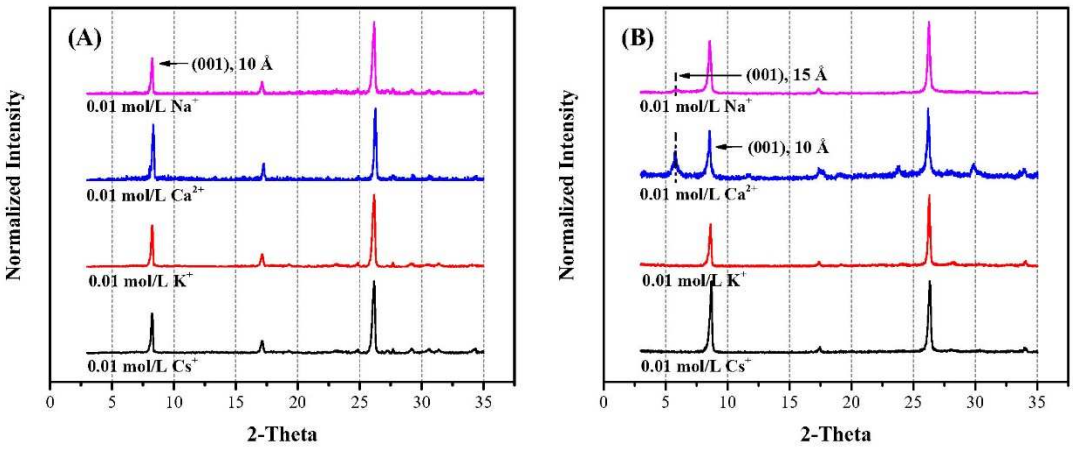

732

733 Fig. 3. Effect of the background electrolyte on the structures of Eu(III)-loaded (A)

734 muscovite and (B) phlogopite (T = 25±1 □, s/l = 1.0 g/L, $[Eu(III)]_{initial}$ = 5.0×10^{-5}

735 mol/L, pH = 5.3±0.1, 48 h).

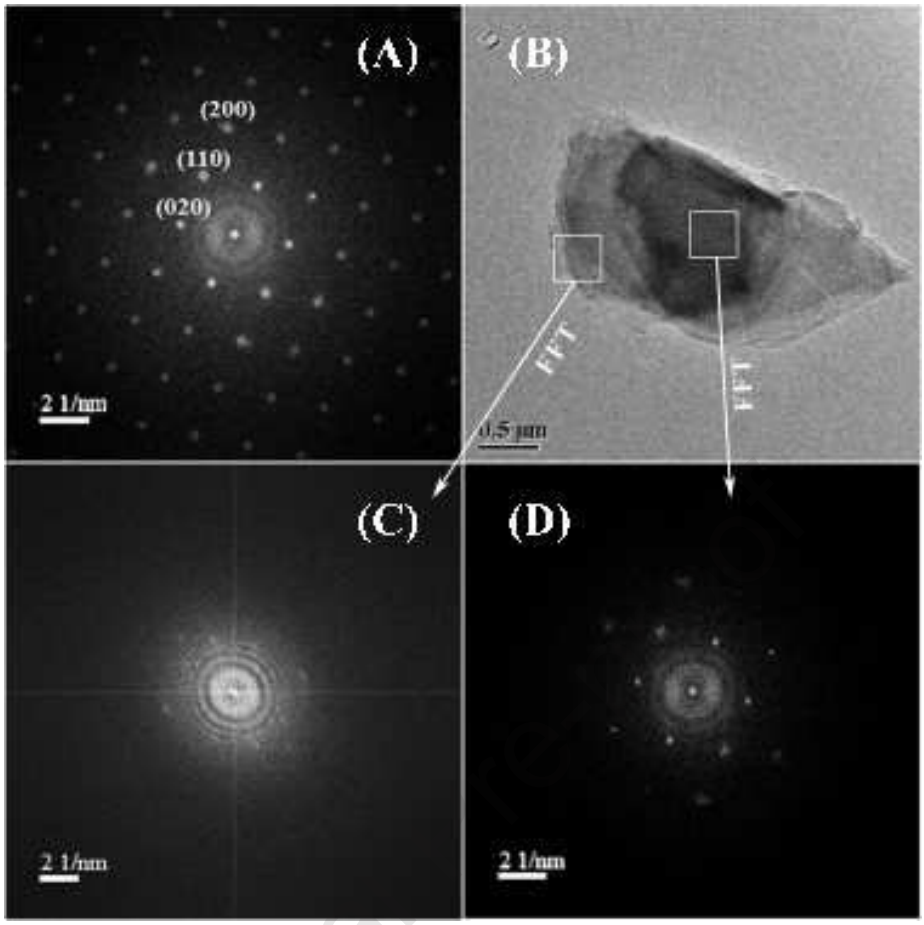

736

737 Fig. 4. The TEM images of Eu(III)-loaded micas. (A) The SAED of muscovite and (B)

738 TEM of phlogopite with (C and D) the magnified FFT images (SAED) indicated by

739 the white square. (T = 25±1 □, s/l = 1.0 g/L, I = 0.01 mol/L NaCl, $[Eu(III)]_{initial}$ =

740 1.0×10^{-4} mol/L, pH = 5.3±0.1, 48 h)

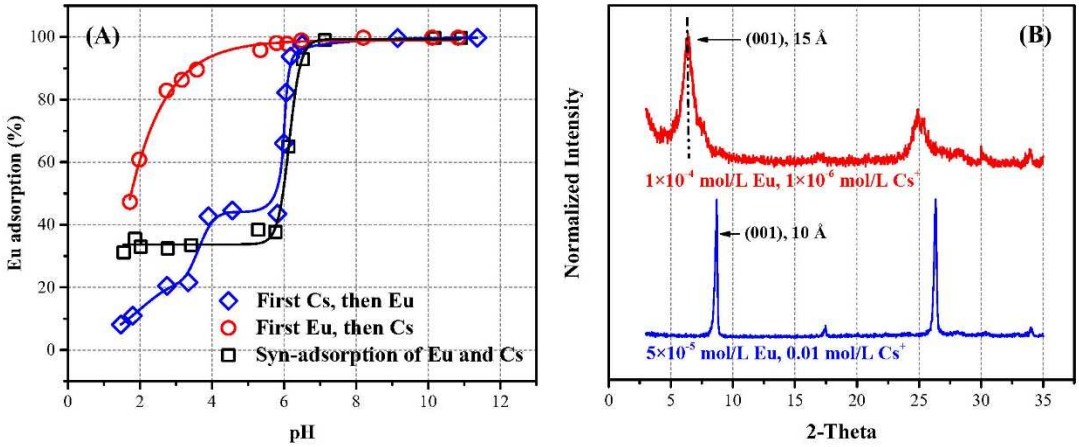

741

742 Fig. 5. Effect of Cs^+ on Eu(III) adsorption by phlogopite (T = 25±1 □, s/l = 1.0 g/L).

743 (A) Eu(III) adsorption in different reaction sequences ($[Eu(III)]_{initial}$ = 5.0×10^{-5} mol/L,

744 I = 0.01 mol/L CsCl) and (B) XRD patterns of the Eu(III)-loaded phlogopite in

745 different [Eu(III)]-to-[Cs^+] ratio at pH 5.3.

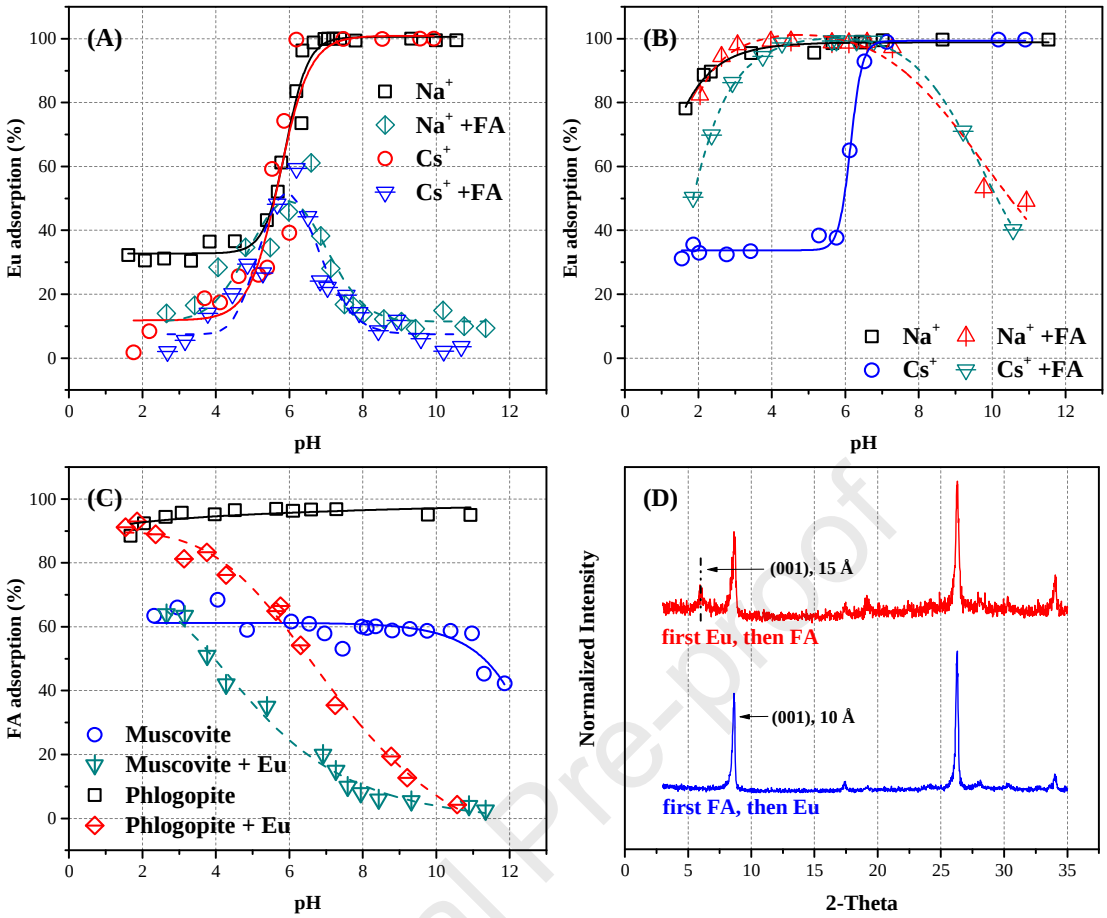

746

747 Fig. 6. Effect of the FA on Eu(III) adsorption by micas (T = 25±1 □, s/l = 1.0 g/L, I =

748 0.01 mol/L NaCl or CsCl, $[Eu(III)]_{initial}$ = 5.0×10^{-5} mol/L, $[FA]_{initial}$ = 50.0 mg/L, 48

749 h). (A) Eu(III) adsorption on muscovite, (B) Eu(III) adsorption on phlogopite, (C) FA

750 adsorption on muscovite and phlogopite in the absence and presence of Eu(III), and

751 (D) effect of reaction sequences of Eu(III) and FA on the structures of phlogopite

752 samples at pH 5.3.

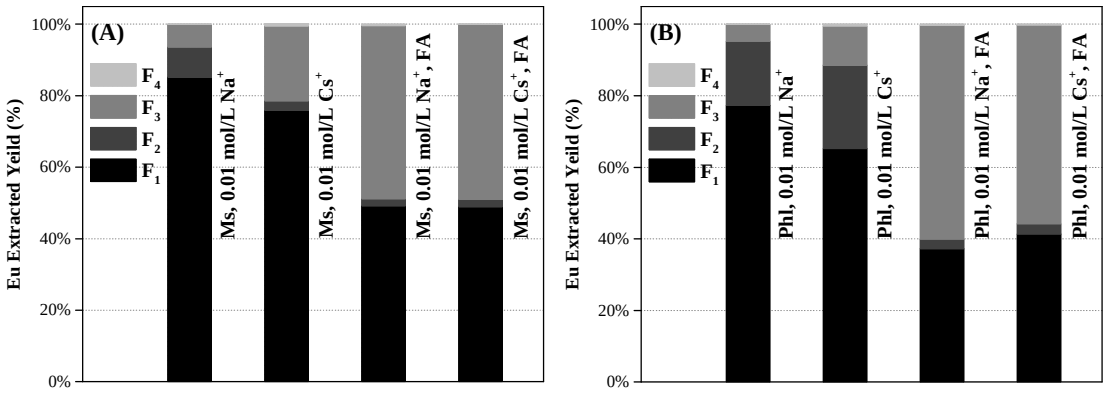

753

754 Fig. 7. Sequential extraction of Eu(III) from (A) Eu-loaded muscovite (Ms) samples

755 and (B) Eu-loaded phlogopite (Phl) samples (T = 25±1 □, s/l = 1.0 g/L, I = 0.01

756 mol/L NaCl or CsCl, $[Eu(III)]_{initial}$ = 5.0×10^{-5} mol/L, $[FA]_{initial}$ = 50.0 mg/L, pH =

757 5.3±0.1). F_1: extracted by 1.0 mol/L $CaCl_2$; F_2: extracted by 1.0 mol/L NH_4OAc; F_3:

758 extracted by HNO_3 of pH 2; F_4: residual fraction.

CRediT author statement

Hanyu WU: Conceptualization, Formal analysis, Investigation, Resources, Data Curation, Writing- Original Draft, Writing- Review & Editing, Visualization, Supervision, Project administration, Funding acquisition

Jie CHEN: Validation, Formal analysis, Investigation, Data Curation, Visualization

Zengbo SU: Validation, Formal analysis, Investigation, Data Curation, Visualization

Bin MA: Writing- Review & Editing, Project administration

Yizhe JI: Investigation, Project administration

Shuhan LIN: Investigation

Dingfang XU: Data Curation

Mingliang KANG: Resources, Writing- Review & Editing, Supervision, Funding acquisition

Highlights

- Dioctahedral and trioctahedral endmember micas were comparatively studied
- Cs^+ could decrease Eu adsorption capacity of phlogopite to the level of muscovite
- Eu(III) intercalated into interlayer sites of trioctahedral phlogopite
- The extent of interlayer expansion was positively correlated with Eu(III) loadings
- FA occupied interlayer sites of phlogopite and competed with interlayer Eu(III)